## *Supplementary Methods*

### 1 Adjusting of meteorological inputs

Temperature was adjusted at the Hunza basin scale using a deviation function, which resulted in a range of ±1°C between HAR temperature and station temperature, with a correlation coefficient of 0.98. We adjusted precipitation use a water balance approach, which will be elucidated in further detail below. Due to the lack of observations for other variables, no further processing was conducted in this study.

Numerous research endeavors have elucidated notable biases in precipitation observations within and in the vicinity of the Hunza river basin. For instance, Winiger et al. (2005) discovered a noteworthy discrepancy, with precipitation at altitudes surpassing 5000 m exhibiting sixfold or more intensity compared to lower altitudes, as deduced from station observations. Similarly, Tahir et al. (2011) ascertained a dissimilarity between runoff and observed precipitation, with Dainyor station recording a runoff of 750 mm/yr but a mere 100 mm/yr of observed precipitation. This asymmetry was also discerned in the neighboring region (Immerzeel et al., 2009). To make a more accurate precipitation input for the simulation, we consulted the method proposed by Wortmann et al. (2018) to rectify the precipitation data. This method entails the calibration of precipitation through the calculation of the calibration factor $f_c(H)$, as expressed by the following equation:

$$f_c(H) = (c-1)\exp\left\{-\left[\frac{P_{LR}}{(c-1)*100}\right]^2 * (H - H_{max})^2\right\} + 1 \quad (1)$$

Where $c$ represents the calibration factor, $H_{max}$ represents the maximum elevation at which precipitation occurs, $P_{LR}$ signifies the elevation correction factor for precipitation. These parameters are determined using the linear relationship proposed by Immerzeel et al. (2012), and the range of values for the determination is derived from existing studies. The linear relationship can be expressed as follows:

'H_ref' denotes the reference elevation, which corresponds to the elevation at which the observed precipitation closely matches the actual precipitation.

$$\begin{cases} P_T = P_{HAR} * \left[1 + \left(H - H_{ref}\right) * P_{LR} * 0.01\right] & H_{ref} < H < H_{max} \\ P_T = P_{HAR} * \left[1 + \left(\left(H_{max} - H_{ref}\right) + \left(H_{max} - H\right)\right) * P_{LR} * 0.01\right] & H > H_{max} \end{cases} \quad (2)$$

Where $H_{ref}$ denotes the reference elevation, which corresponds to the elevation at which the observed precipitation closely matches the actual precipitation. $P_{HAR}$ and $P_T$ represent HAR precipitation and calibrated precipitation. We determine $H_{max}$ and $P_{LR}$ by approximating the calculated $P_r$ based on the water balance equation (Eq. 3) (Figure SM1), with the range of values for $H_{max}$ and $P_{LR}$ referencing the priori studies. In the Eq.3, $ET$ uses MODIS evapotranspiration products, $R$ takes the runoff from the watershed outlet observation station (Dainyor station), and TWS takes the average of GLDAS and GRACE soluitions.

$$P_r - ET - R - TWS = 0 \quad (3)$$

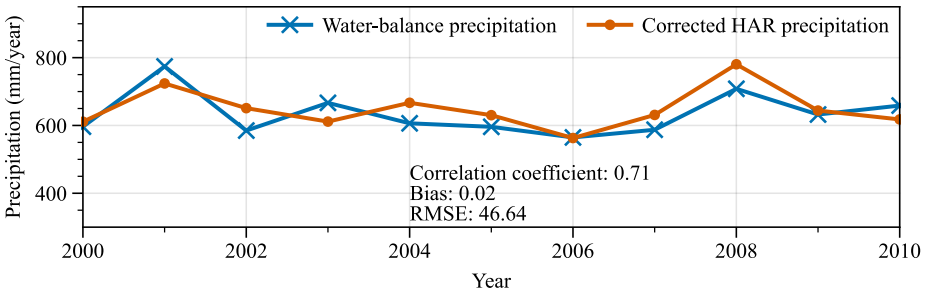


**Figure SM 1** Comparison between corrected precipitation and precipitation calculated by water balance equation.

**2 Downscaling of the model inputs**

In order to achieve the desired level of precision for mass balance simulation on a glacier scale, this study downscaled HAR reanalysis data from 10 km to 300 m by using statistical methods. Special attention was given to the impacts of topography, slope, and aspect on meteorological factors during this process. The SRTM DEM with a spatial resolution of approximately 30 meters was utilized to obtain topographic features. In order to effectively represent topographical features on a glacier scale while maintaining optimal computational efficiency during the energy balance simulation process, the target grid size was set at 10 times the SRTM DEM (~300 m).

Based on water balance at basin outlet, the precipitation was first calibrated using remote sensing data and station observations to obtain the altitude gradient lapse rate and maximum precipitation altitude (Supplementary Methods). After calibration, the altitude gradient lapse rate of precipitation throughout the Hunza river basin was determined to be 0.18%/m. The maximum precipitation altitude of the Batura glacier was 4900 m. Then, the precipitation was downscaled at a resolution of 300 m for the Batura glacier by applying the Eq.1 provided in the Supplementary. Incoming shortwave radiation was downscaled by using the radiative transfer equation (Eq.4) on sloping surfaces. The details in solving this equation can be found in publication of Ham (2005). The correlation coefficient of incoming shortwave radiation before and after downscaling is 0.91, with an RMSE of 26, indicating the parameterization-based downscaling enables a more refined representation of spatial characteristics while preserving the original characteristics and trends of the data.

$$R_{gs} = R_b \left( \frac{\cos(\phi)\cos(i) + \sin(\phi)\sin(i)\cos(\gamma - \alpha)}{\cos(\phi)} \right) + R_d \quad (4)$$

In the above equation, $R_d$ represents scattered radiation, which is solved using a modified Gompertz function that quantifies the relationship between horizontal total radiation ($R_{gh}$) and clear sky index (CI) (Wohlfahrt et al., 2016); CI is determined based on radiation duration, while $R_{gh}$ is initialized as $R_{gs}$; $R_b$ denotes direct incident radiation and is calculated by subtracting $R_d$ from $R_{gh}$; $\phi$ and $\gamma$ represent solar zenith angle and azimuth angle respectively, which can be obtained using parameterization schemes proposed by Wohlfahrt et al. (2008); $i$ denotes the angle between the slope and horizontal plane, while $\alpha$ represents the azimuth angle of the slope.

Temperature, relative humidity, wind speed, and air pressure were downscaled using altitude gradient lapse rates obtained from HAR data. Cloud cover was downscaled refer to the scheme of ERA5 (Muñoz Sabater, 2019). Owing to the absence of meteorological observations required for

computing altitude gradient lapse rates, the lapse rates over a broader region (Karakoram Mountains), which encompasses the study area, were determined using HAR data to minimize errors. The altitude gradient lapse rate for 2 m air temperature was calculated to be -0.0054 ℃/m, while that for 2 m wind speed was 0.00078 $m*s^{-1}/m$. The rate for 2 m relative humidity was 0.014 %/m, and that for atmospheric pressure was -0.044 hPa/m.

### *Supplementary Tables*

**Table S1** The primary parameters in the energy balance model.

| Parameter | Value | Parameter | Value | Parameter | Value |
|---|---|---|---|---|---|
| fresh snow albedo | 0.88 | surface roughness length for fresh snow | 0.24 mm | thickness of snow layers | 2 cm |
| firn albedo | 0.53 | surface roughness length for aged snow | 6 mm | thickness of glacier ice layers | 50 cm |
| ice albedo | 0.3 | surface roughness length for ice | 2.5 mm | Surface emission coefficient | 0.97 |
| albedo timescale | 13 days | firn density | 550 $kg/m^3$ | melting temperature | 273.15 K |
| albedo depth scale | 3 cm | ice density | 875 $kg/m^3$ | bottom temperature | 265.15 K |
| Temperature threshold of rain/snow ratio | [-0.5~4.5℃] | density of freshly fallen snow | 250 $kg/m^3$ | | |

**Table S2** The key parameters in the energy balance of debris.

| Parameter | Value | Unit | Explanation |
|---|---|---|---|
| debris aerodynamic roughness length for debris | 0.016 | m | – |
| Debris thermal conductivity | 0.76 | $W\ m^{-1}\ K^{-1}$ | – |
| debris density | 1496 | $kg\ m^{-3}$ | – |
| debris specific heat capacity | 900 | $J\ kg^{-1}\ m^{-3}$ | – |
| debris volumetric heat capacity | 1418208 | $J\ m^{-3}\ K^{-1}$ | – |
| ice emissivity | 0.94 | – | – |
| debris albedo | 0.13 | – | When debris is covered with snow, the albedo is set as the albedo of snow of which is parameterized by |

| | | | |
|---|---|---|---|
| | | | using the evolution scheme of COSIPY |
| debris layer thickness | 0.01 | m | When there are fewer than 10 layers, it is adjusted to have 10 layers with a thickness of total thickness divided by 10 for each layer. |

## *Supplementary Figures*

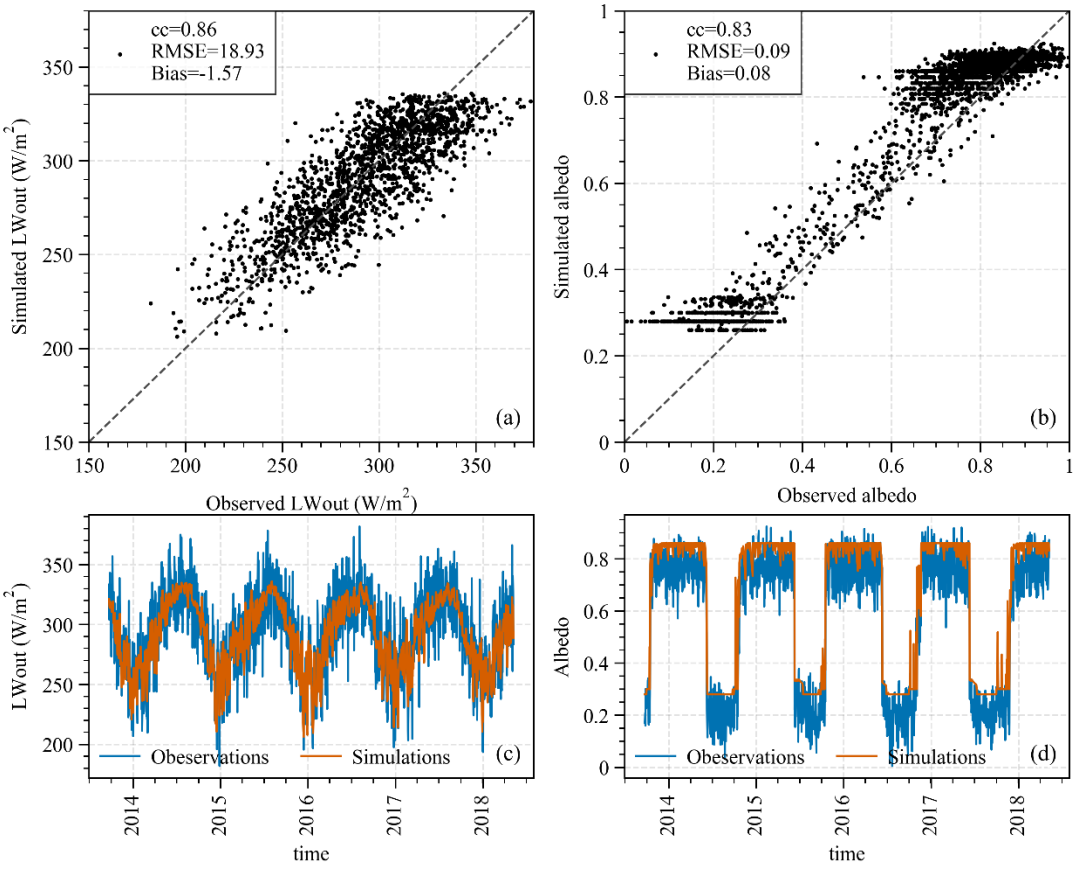


**Figure S1** Comparison of observed and simulated (a), (c) outgoing longwave radiation and (b), (d) albedo at AWS1.

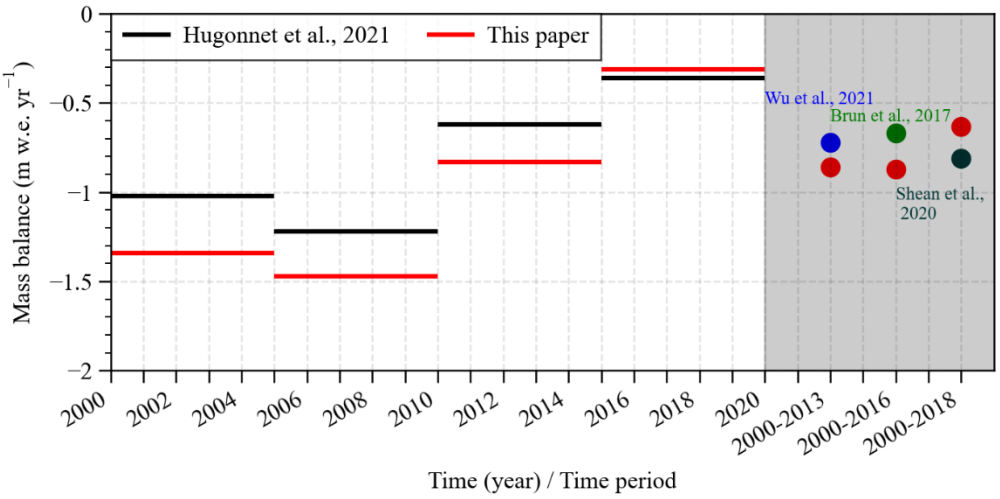


**Figure S2** Comparison of simulated and geodetic mass balance over different time periods.

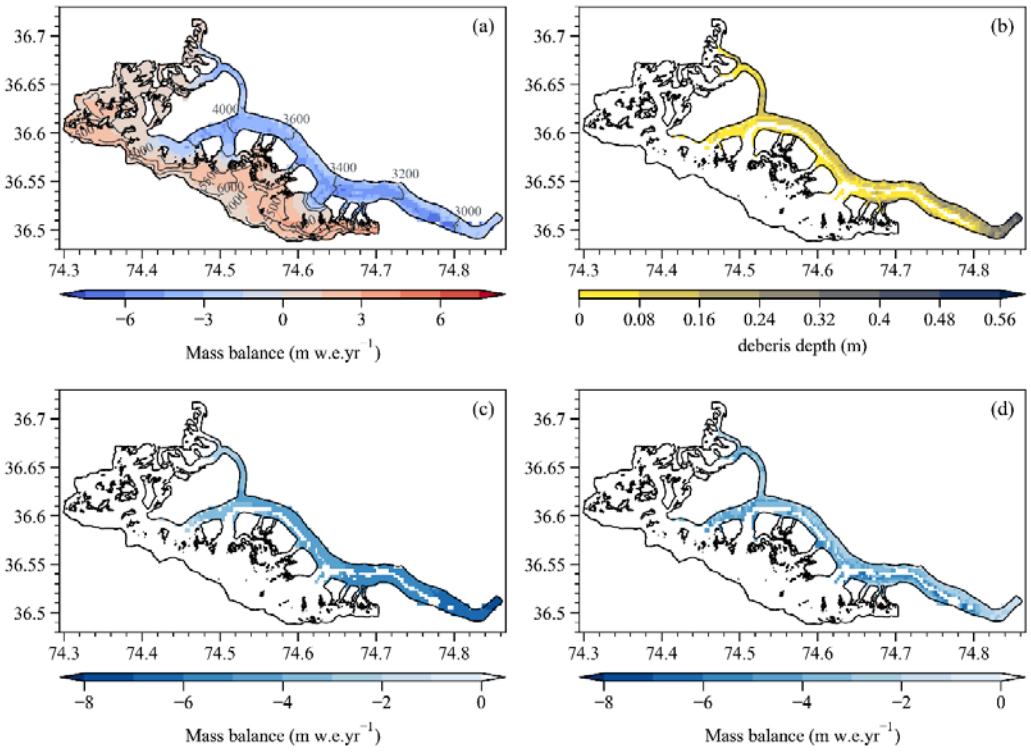


**Figure S3** Spatially-distributed mass balance in Batura glacier. (a) Annual mass balance; (b) Debris thickness; (c) Annual ablation with no debris cover; (d) Annual ablation with full debris cover.

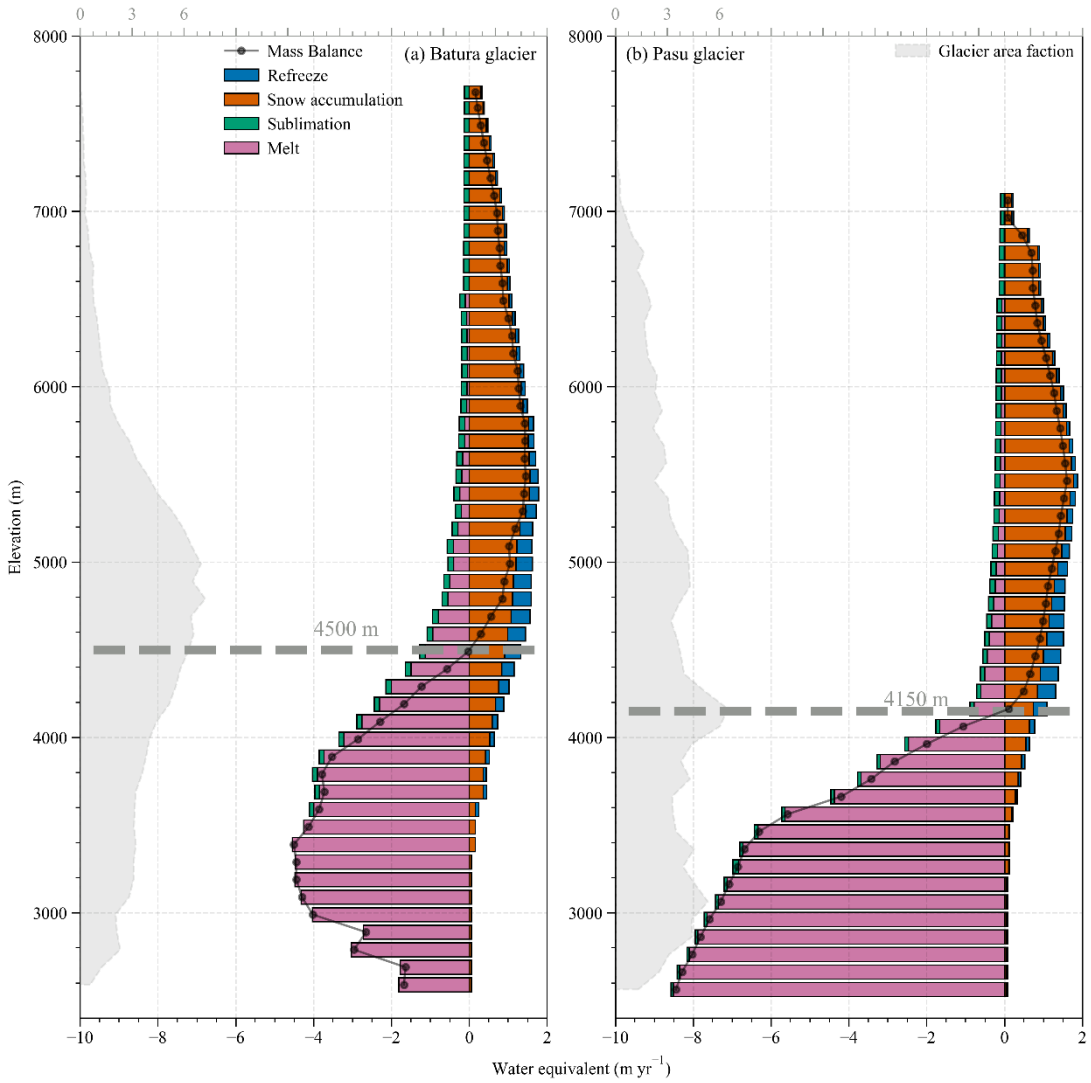


**Figure S4** Characteristics of altitude gradient of components in mass balance. (a) Batura Glacier; (b) Pasu Glacier. The glacier ratio fraction (%) represents proportion of the glacier area in each elevation zone to total area of the glacier.

References

Ham, J.M., 2005. Useful Equations and Tables in Micrometeorology, Micrometeorology in Agricultural Systems, pp. 533-560.

Immerzeel, W.W., Pellicciotti, F. and Shrestha, A.B., 2012. Glaciers as a Proxy to Quantify the Spatial Distribution of Precipitation in the Hunza Basin. Mountain Research and Development, 32(1): 30-38.

Immerzeel, W.W., Rutten, M.M. and Droogers, P., 2009. Spatial downscaling of TRMM precipitation using vegetative response on the Iberian Peninsula. Remote Sensing of Environment, 113(2): 362-370.

Muñoz Sabater, J., 2019. ERA5-Land hourly data from 1981 to present. In: C.C.C.S.C.S.C.D.S. (CDS)

(Editor).

Tahir, A.A., Chevallier, P., Arnaud, Y. and Ahmad, B., 2011. Snow cover dynamics and hydrological regime of the Hunza River basin, Karakoram Range, Northern Pakistan. Hydrology and Earth System Sciences, 15(7): 2275-2290.

Winiger, M., Gumpert, M. and Yamout, H., 2005. Karakorum-Hindukush-western Himalaya: assessing high-altitude water resources. Hydrological Processes, 19(12): 2329-2338.

Wohlfahrt, G., Hammerle, A., Haslwanter, A., Bahn, M., Tappeiner, U. and Cernusca, A., 2008. Disentangling leaf area and environmental effects on the response of the net ecosystem CO2 exchange to diffuse radiation. Geophys Res Lett, 35(16).

Wohlfahrt, G., Hammerle, A., Niedrist, G., Scholz, K., Tomelleri, E. and Zhao, P., 2016. On the energy balance closure and net radiation in complex terrain. Agric For Meteorol, 226-227: 37-49.

Wortmann, M., Bolch, T., Menz, C., Tong, J. and Krysanova, V., 2018. Comparison and Correction of High-Mountain Precipitation Data Based on Glacio-Hydrological Modeling in the Tarim River Headwaters (High Asia). Journal of Hydrometeorology, 19(5): 777-801.